Wavepacket Modeling of the Jet Noise Source

Dimitri Papamoschou*
University of California, Irvine, CA 92697, USA

This study is motivated by the need for physical models for the jet noise source to be used in practical noise prediction schemes for propulsion-airframe integration concepts. The basis for the source model is an amplitude-modulated traveling wave - the wavepacket. The source is parameterized and the parameters are determined by minimizing the difference between the modeled and experimental sound intensity distributions in the far field. Even though the pressure signal that reaches the far field is highly filtered, sufficient information is available to construct a wavepacket with reasonable physical characteristics. A simple stochastic extension of this concept shows a connection between the shape of the far-field sound pressure level spectrum and the emission polar angle. It suggests that the broadening of the spectrum with increasing polar angle from the downstream axis can be explained on the basis of a single noise source (the wavepacket), rather than the prevailing model of two distinct noise sources, one coherent and the other incoherent.

I. Introduction

The study of the noise radiated from turbulent jets was significantly impacted by the experiments of McLaughlin *et al.*[1,2] on the turbulent structure and acoustic radiation of low-Reynolds number supersonic jets. These experiments generated the first direct evidence that peak sound radiation is connected to instability waves at the boundary of the jet. Thus, they provided support for emerging theories on supersonic jet noise, notably that of Tam[3], which connected the emission of directional waves (Mach waves) to the shear layer instability. Later works by McLaughlin and co-workers demonstrated that the instability-wave generation of sound is not restricted to low-Reynolds number jets and persists to high Reynolds numbers[4,5]. One can draw parallels between this discovery and the Caltech shear-layer experiments of Brown and Roshko[6], where it was determined that coherent structures persist, and dominate turbulent mixing, up to high Reynolds numbers. Today it is widely accepted that the peak noise radiated from turbulent jets, subsonic and supersonic, comes from the large-scale coherent structures in the jet flow. This paper develops concepts whose roots can be traced back to the seminal studies of Professor Dennis K. McLaughlin.

The work presented here is motivated by the need of the aerospace industry for low-order models of the jet noise source that can be used in the acoustic assessment of propulsion-airframe integration. Even though the jet noise source, and resulting emission, can be computed from first principles, such computations are very expensive and time consuming. What is sought here is a simple equivalent source model that captures the salient physics of the flow and reproduces faithfully the acoustic field. Further, the acoustic data used to calibrate and validate the model could be limited. For example, in the development of next-generation tools for aircraft noise prediction, the only widely available data for determining the jet noise source are far-field autospectra at a range of polar and azimuth angles[7]. For subsonic jets, the information propagated to the far field is very limited, which presents a challenge in this type of determination of the noise source.

The intention of this paper is to develop approaches for the determination of a physically meaningful jet noise source model based on the minimal information propagated to the far field. The principal component of this approach is the wavepacket model, i.e., an amplitude-modulated traveling wave of pressure prescribed on a cylindrical surface surrounding the jet and in the linear pressure field. An attribute of this formulation is that it allows the use of linear propagation and scattering tools, such as the boundary element method, to compute the acoustics of propulsion-airframe integration. A preliminary example of such

* Professor, Department of Mechanical and Aerospace Engineering, dpapamos@uci.edu.

computation can be found in Ref.8. In the present paper, it will be shown that the information propagated to the far field may be sufficient to estimate not only the overall shape of the wavepacket but also the content of its dominant azimuthal (helical) modes. In particular, a strong connection is made between the directivity of jet noise and the azimuthal mode content of the source.

An additional aspect of this study is re-examination the commonly held view that the broadening of the sound pressure level (SPL) spectrum with increasing polar angle from the jet axis indicates two distinct noise sources, a "coherent" source radiating a small angles, and an omnidirectional "incoherent" source. This concept has found wide acceptance in the aerocoustic community, and an overview of its rationale can be found in Ref. 9. Indeed, there is significant circumstantial evidence to support the two-source model. On other hand, there is no conclusive proof that the shock-free turbulent jet has two distinct, independent, noise sources.

This paper refines and expands on ideas originally presented in Ref. 10. We adopt a holistic view of the far-field spectrum, in the form of a contour map on the Strouhal number (Sr) - polar angle (θ) plane. This is shown in Fig.1 for a Mach 0.9 cold air jet, using acoustic data measured in the UC Irvine Jet Aeroacoustics Facility[11]. We note that the peak SPL level occurs at small angles and Sr~0.1. Plotted against frequency, the spectrum is peaky at small polar angles and broader at large angles. The direction of peak emission increases considerably with increasing frequency, an important trend that deserves attention. Generally speaking, broadening of the spectrum indicates weaker temporal coherence of the acoustic field. Connecting this to the temporal or spatial coherence of the source is not straight-forward. A spatially-incoherent source field (e.g., a set of uncorrelated monopoles) can generate an acoustic field with finite spatial coherence[11,12]. Further, we should allow for the possibility that the broadening of the spectrum with angle may be related to the propagation of sound from a distributed and directive source. Indeed, it will be shown that a single jet noise source model based on the wavepacket alone will capture the basic features of the spectrum of Fig.1.

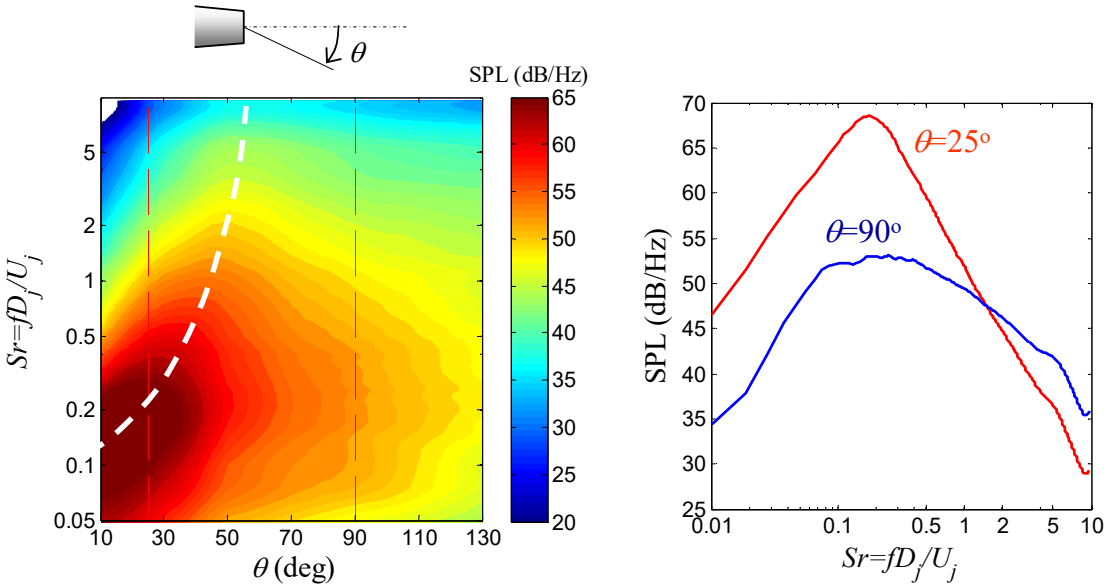

Fig. 1 Spectrum of the far-field sound pressure level for a Mach 0.9 cold jet. Contour map on the left plots the SPL versus polar angle and Strouhal number; white dashed line indicates polar direction of peak emission. Plot on the right shows the SPL versus Strouhal number at θ=25° and 90°.

The wavepacket model development of this paper builds on the foundational works by Tam and Burton[13], Crighton and Huerre[14], Avital *et al.*[15], and Morris[16]. There is increasing experimental evidence that the peak noise radiation in subsonic and supersonic jets is linked to an instability-wave mechanism[17-

[20]. Here we seek to understand and model the wavepacket noise source based on far-field intensity measurements, expanding on earlier related studies of our group[8].

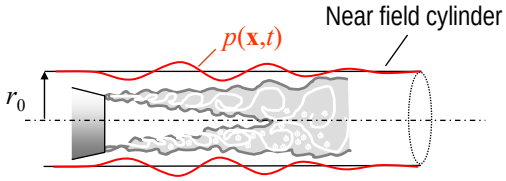

Fig. 2 Wavepacket concept.

Following the analysis by Morris[16], we consider a cylindrical surface surrounding a turbulent jet, as depicted in Fig. 2. The radius r_0 of the surface is sufficiently close to the jet to sense both the radiating and non-radiating (hydrodynamic) components of the turbulent pressure fluctuations. It is assumed that the cylinder is in a stationary ambient medium surrounding the jet.

The generic wavepacket model is depicted in Fig.3 and the coordinate systems used in the analysis that follows are shown in Fig.4. The paper starts with a deterministic noise source model based on the wavepacket ansatz. The model is then generalized to a stochastic perturbation. The test flow is a cold round air jet with Mach number M_j=0.9 and velocity U_j=285 m/s, issuing from a nozzle with diameter D_j=21.8 mm. The Reynolds number is 5.6 ×10^5. The frequency f is presented in the non-dimensional form of Strouhal number $Sr=fD_j/U_j$.

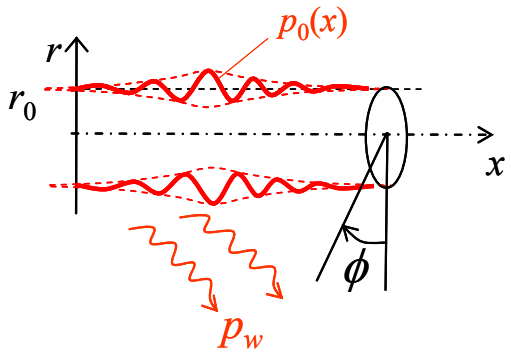

Fig. 3 Wavepacket model of jet noise.

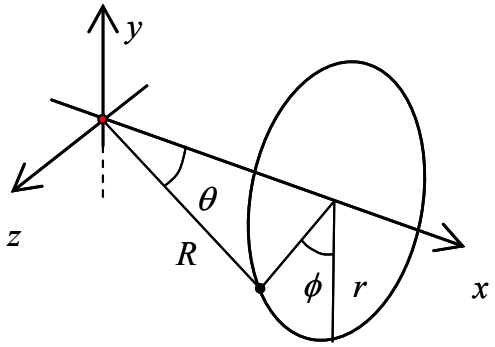

Fig. 4 Cartesian (x, y, z) , polar (x ,r, ϕ), and spherical (R,θ, ϕ) coordinate systems.

II. Deterministic Source Model

A. Elementary Model

On the cylinder surface $r=r_0$ we prescribe the pressure perturbation

$$p_w(n,r_0,x,\varphi,t) = p_0(x)e^{-i\omega t+in\phi} \tag{1}$$

where n denotes the helical mode and ϕ is the azimuthal angle. The shape $p_0(x)$ will take the form $p_0(x) = A(x)e^{i\alpha x}$, with $A(x)$ an amplification-decay envelope that represents the axial coherence length scale, and α the instability wavenumber. Denoting the spatial Fourier transform of $p_0(x)$ as $\hat{p}_0(k)$, the solution for $r \geq r_0$ is[16]

$$p_w(n,r,x,\varphi,t) = \frac{1}{2\pi} e^{-i\omega t + in\phi} \int_{-\infty}^{\infty} \hat{p}_0(k) \frac{H_n^{(1)}(\lambda r)}{H_n^{(1)}(\lambda r_0)} e^{ikx} dk$$
$$\lambda = \left[\left(\frac{\omega}{a_\infty} \right)^2 - k^2 \right]^{1/2}, \quad -\frac{\pi}{2} < \arg(\lambda) < \frac{\pi}{2} \tag{2}$$

where $H_n^{(1)}$ is the Hankel function of the first kind of order n, and λ is the radial wavenumber. Equation 2 is the exact solution to the linearized problem, valid everywhere for $r \geq r_0$. An important aspect of the pressure field generated by the wavepacket is that it has a radiative (supersonic) component and a decaying (subsonic) component. The decaying, or hydrodynamic, component involves phase speeds that are subsonic, $|\omega/k| < a_\infty$ or $|k| > \omega/a_\infty$:

$$p_{w,sub}(n,r,x,\varphi,t) = \frac{1}{2\pi} e^{-i\omega t + in\phi} \int_{|k|>\omega/a_\infty} \hat{p}_0(k) \frac{H_n^{(1)}(\lambda r)}{H_n^{(1)}(\lambda r_0)} e^{ikx} dk \tag{3a}$$

The radiating component involves phase speeds that are sonic or supersonic, $|k| \leq \omega/a_\infty$:

$$p_{w,\sup}(n,r,x,\varphi,t) = \frac{1}{2\pi} e^{-i\omega t + in\phi} \int_{-\omega/a_\infty}^{\omega/a_\infty} \hat{p}_0(k) \frac{H_n^{(1)}(\lambda r)}{H_n^{(1)}(\lambda r_0)} e^{ikx} dk \tag{3b}$$

From Eq.3b, using the convolution property of the Fourier transform, we obtain an expression for the part of $p_0(x)$ that radiates to the far field:

$$p_{0,\sup}(x) = \frac{1}{\pi} \int_{-\infty}^{\infty} \frac{p_0(\xi)}{x-\xi} \sin\left[\frac{\omega}{a_\infty} (x-\xi) \right] d\xi \tag{4}$$

The far-field approximation of Eq.2 is[16]

$$p_{w,far}(n,R,\theta,\varphi,t) = -\frac{i}{\pi R} \frac{\hat{p}_0\left(\frac{\omega}{a_\infty} \cos\theta \right)}{H_n^{(1)}\left(\frac{\omega}{a_\infty} r_0 \sin\theta \right)} e^{i\omega R/a_\infty} e^{-i\omega t + in\phi} \tag{5}$$

where R is the distance of the observer from the origin and θ is the polar angle from the downstream wavepacket (jet) axis. The modulus squared of Eq.5 yields the variance of the far-field pressure:

$$S_{w,far}(n,R,\theta,\omega) = \frac{1}{(\pi R)^2} \left| \frac{\hat{p}_0\left(\frac{\omega}{a_\infty} \cos\theta \right)}{H_n^{(1)}\left(\frac{\omega}{a_\infty} r_0 \sin\theta \right)} \right|^2 \tag{6}$$

B. Self-Similar Model

This is a special implementation of the wavepacket model, applicable to the shear layer surrounding the potential core of the jet where we expect a constant convective velocity U_c and some aspects of self-similar behavior. Specifically we expect that the axial extent of the wavepacket envelope (or coherence length scale) will be inversely proportional to the frequency ω, or instability wavenumber $\alpha = \omega/U_c$. Whereas in the original formulation of $p_0(x)$ in Eq.1 we imposed the variation

$$p_0(x) = A(x) e^{i\alpha x}$$

now we are stating

$$p_0(x) = A(\alpha x)e^{i\alpha x}$$

In other words, we replace $p_0(x)$ by the self-similar form $P_0(\alpha x)= P_0(\omega x/U_c)$. There is experimental evidence by Chan[21] that this type of self-similar formulation collapses the pressure distributions in the shear layer of the jet. Besides its physical basis, this formulation helps clarify the salient variables in the propagation process. In turn, this enables an identification scheme for the dominant helical mode n as a function of frequency ω, a key step towards developing a model that can be applied for all frequencies at once. In the elementary wavepacket analysis of Section II.A, the pressure on the cylinder $r=r_0$ was prescribed as

$$p_w(n, r_0, x, \varphi, t) = p_0(x)e^{-i\omega t+in\phi}$$

We now revise this formulation as follows:

$$p_w(r_0, x, \varphi, t) = \varepsilon(\omega)P_0(\omega x / U_c)e^{-i\omega t+in(\omega)\phi} \tag{7}$$

where $\varepsilon(\omega)$ is an empirically-determined amplitude and the helical mode follows a given relationship with frequency, $n=n(\omega)$. The function $P_0(\omega x/U_c)$ is implied to be a universal function for a given jet. It is easy to show that

$$\hat{p}_0(k) = U_c \frac{\varepsilon(\omega)}{\omega} \hat{P}_0(kU_c / \omega) \tag{8}$$

Considering the far-field solution for the simple wavepacket, the pressure (Eq.5) takes the form

$$p_{w,far} = \varepsilon(\omega)\frac{U_c}{i\omega\pi R}\frac{\hat{P}_0\left(M_c\cos\theta\right)}{H^{(1)}_{n(\omega)}\left(\frac{\omega}{a_\infty}r_0\sin\theta\right)}e^{i\omega R/a_\infty}e^{-i\omega t+in(\omega)\phi} \tag{9}$$

and the variance (Eq.6) becomes

$$S_{w,far}(R,\theta,\omega) = U_c^2\frac{\varepsilon^2(\omega)}{(\pi R\omega)^2}\left|\frac{\hat{P}_0\left(M_c\cos\theta\right)}{H^{(1)}_{n(\omega)}\left(\frac{\omega}{a_\infty}r_0\sin\theta\right)}\right|^2 \tag{10}$$

where $M_c=U_c/a_\infty$ is the convective Mach number, which is a constant for the shear layers surrounding the potential core of the jet. In Eq.10 the only coupling between frequency and polar angle comes from the Hankel-function term in the denominator. This has implications on the determination of the helical mode content of the stochastic version of this model.

C. Combination with Monopole

The wavepacket model by itself may be unable to capture the directivity of jet noise at large polar angles from the jet axis. It is therefore necessary to combine it with a secondary noise source that has omnidirectional character. This source may represent localized sources, near the nozzle exit, that cannot be characterized by a traveling wave. In addition, it may be used as representation of sound emitted by isotropic turbulence, whose propagation is nearly spherical[22]. This secondary noise source is selected here to be a monopole with acoustic field

$$p_m(R,t) = \frac{Q}{R}e^{-i\omega t+ikR} \tag{11}$$

where Q denotes the monopole strength. The wavepacket and monopole sources are taken to be uncorrelated to each other, so the variance of the combined field is the summation of the individual variances. The modeled variance in the far field thus takes the form:

$$S_{\text{mod}} = S_{w,far} + \frac{Q^2}{R^2} \tag{12}$$

where $S_{w,far}$ is given by Eq. 6 for the elementary wavepacket model or Eq. 10 for the self-similar wavepacket model. For the jets considered in this study, the monopole strength will comprise a small fraction of the total source strength.

III. Stochastic Source Model

The actual jet noise source is, of course, random. The stochastic nature of the jet noise source is now addressed at a simplified level.

A. Self-Similar Wavepacket

We construct a stochastic extension of the self-similar wavepacket. In the analysis that follows, the brackets < > denote the expected value or ensemble average. We envision the pressure perturbation on the cylinder $r=r_0$ consisting of a superposition of self-similar wavepackets at a spectrum of frequencies:

$$p(x,r_0,\varphi,t)=\int_{-\infty}^{\infty}\varepsilon(\omega)\,P_0\left(\frac{\omega\left(x-x_0(\omega)\right)}{U_c}\right)\exp\left[-i\omega t+in(\omega)\phi\right]d\omega \tag{13}$$

Each elemental wavepacket has random complex amplitude $\varepsilon(\omega)$ and random origin $x_0(\omega)$. The two random variables are independent. The helical mode n is a deterministic, integer function of frequency. As assumed previously, the function $P_0(x)$ is a universal function for a given jet. In the model of Eq. 13 we consider only one helical mode at each frequency, whereas in reality the pressure perturbation may contain a series of modes. The wavepackets are mutually uncorrelated, $<\varepsilon(\omega_1)\,\varepsilon(\omega_2)>=0$ for $\omega_1\neq\omega_2$.

Since we are interested in the far field ($|x_0|<<R$), and there is no interference between any of the wavepackets, their axial origins x_0 are irrelevant to the far-field emission and therefore we do not need to address them. However, this would not be true if we were to construct a solution for the near field. A full stochastic model would include a probability density function for distribution of $x_0(\omega)$.

Knowing the solution for each individual contribution to the integral from Eq.13, we construct the solution for the far field pressure:

$$p(R,\theta,\phi,t)=-i\int_{-\infty}^{\infty}\varepsilon(\omega)\;\frac{U_c}{\pi R\omega}\frac{\hat{P}_0\left(M_c\cos\theta\right)}{H^{(1)}_{n(\omega)}\left(\frac{\omega}{a_\infty}r_0\sin\theta\right)}\;e^{i\omega R/a_\infty}e^{-i\omega t+in(\omega)\phi}d\omega \tag{14}$$

Denoting for convenience

$$\Psi(\omega,\theta)=\frac{U_c}{\pi R\omega}\frac{\hat{P}_0\left(M_c\cos\theta\right)}{H^{(1)}_{n(\omega)}\left(\frac{\omega}{a_\infty}r_0\sin\theta\right)} \tag{15}$$

the far field variance is

$$\left\langle pp^*\right\rangle=\int_{-\infty}^{\infty}\int_{-\infty}^{\infty}\left\langle\varepsilon(\omega)\,\varepsilon^*(\omega')\right\rangle\Psi(\theta,\omega)\Psi^*(\theta,\omega')e^{-i(\omega-\omega')(t-R/a_\infty)}e^{i[n(\omega)-n(\omega')]\phi}d\omega d\omega' \tag{16}$$

where * denotes the complex conjugate. Invoking the orthogonality of the wavepackets in the form

$$\left\langle\varepsilon(\omega)\,\varepsilon^*(\omega')\right\rangle=\frac{E(\omega)}{2\pi}\delta(\omega-\omega'), \tag{17}$$

with $E(\omega)$ being an empirical function and δ the Dirac delta function, the far-field variance becomes

$$\left\langle pp^*\right\rangle=\frac{1}{2\pi}\int_{-\infty}^{\infty}E(\omega)\left|\Psi(\theta,\omega)\right|^2d\omega \tag{18}$$

From Parseval's theorem, we recognize the integrand as the spectral density and write

$$S_w(R,\theta,\omega) = E(\omega)\left|\Psi(\theta,\omega)\right|^2 = U_c^2 \frac{E(\omega)}{(\pi R\omega)^2}\left|\frac{\hat{P}_0(M_c\cos\theta)}{H^{(1)}_{n(\omega)}\left(\frac{\omega}{a_\infty} r_0 \sin\theta\right)}\right|^2 \tag{19}$$

We obtain essentially the same result as for the deterministic solution, Eq. 10. We note again that the coupling of frequency and polar angle comes solely from the Hankel-function term in the denominator.

B. Combination with Monopole

Considering a monopole of random real strength $q(\omega)$ such that

$$\left\langle q(\omega)\, q(\omega')\right\rangle = Q^2(\omega)\delta(\omega-\omega'), \tag{20}$$

and assuming that the monopole is uncorrelated with the wavepacket, it is evident that the combined spectral density is

$$S_{\text{mod}} = S_{w,\,far} + \frac{Q^2}{R^2} \tag{21}$$

thus recovering the form of Eq.12.

IV. Source Model Parameterization

The noise source parameterization is based solely on far-field intensity data, such as the spectrum of Fig.1. This is motivated by the practical consideration that the vast majority of experimental studies on jet noise have produced only intensity data. Even though such an approach may seem limited, there are features of the noise spectrum, not exploited before, that provide significant guidance for characterizing the noise source. Two parameterization schemes are presented. The first scheme involves parameterization at fixed frequency and is primarily applicable to the deterministic noise model, although it can also be seen as an elementary building block for the stochastic model. The second, so-called global scheme, involves parameterization at all frequencies; it is applicable to both the deterministic model and its stochastic counterpart.

A. Parameterization at Fixed Frequency

Approach

Upon selecting a functional form for the wavepacket shape $p_0(x)$ in Eq.1, the wavepacket shape for given frequency ω and helical mode n can be expressed as

$$p_0(x,\mathbf{A})$$

where A_k, k=1,.., K–1, is a vector consisting of K–1 parameters that define the wavepacket shape. The K^{th} parameter is reserved for the monopole strength Q. The parameterization is conducted for a fixed frequency ω and distance R. Having selected a set of parameters, the modeled far-field intensity is given by Eq. 12. The idea is then to select the parameter vector **A** in a way that minimizes the difference between the modeled intensity distribution $S_{\text{mod}}(\theta, n, \mathbf{A})$ and the experimental intensity distribution $S_{\text{exp}}(\theta)$. Realizing that we are interested in matching the *shape* (directivity) of the polar intensity distribution, and not so much its absolute value, we work with the normalized values of the modeled and experimental variances, expressed here as sound pressure levels (units of decibels):

$$L_{\text{mod}}(\theta,n,\mathbf{A}) = 10\log\left(\frac{S_{\text{mod}}(\theta,n,\mathbf{A})}{S_{\text{mod,max}}(n,\mathbf{A})}\right)$$
$$L_{\text{exp}}(\theta) = 10\log\left(\frac{S_{\text{exp}}(\theta)}{S_{\text{exp,max}}}\right) \tag{22}$$

where max denotes the peak value of the polar distribution. The above normalization eliminates the amplitude constant from the minimization process. Once the shape is matched, the absolute levels can be matched through a trivial adjustment of the amplitude.

Cost function

For a given jet flow, the experimental variance distribution (autospectrum) is known at discrete polar angles θ_j, j=1,..,J. We construct the cost function

$$F(\mathbf{A}) = \sqrt{\frac{1}{J}\sum_{j=1}^{J}\left[L_{\text{exp}}(\theta_j) - L_{\text{mod}}(n,\mathbf{A},\theta_j)\right]^2 + \sum_{k=1}^{K} C_k\left(A_k - A_{k,\text{target}}\right)^2} \tag{23}$$

The first term inside the square root represents the standard error between the modeled and experimental sound pressure level distributions. The second term is a penalty function that constrains **A** to within a target value, where C_k is a vector of appropriately chosen penalty coefficients.

In this study the wavepacket axial shape is assigned the form

$$p_0(x) = \tanh(x/b_1)^{p_1}\left\{1-\tanh(x/b_2)^{p_2}\right\}e^{i\alpha x} \tag{24}$$

which was selected as a promising function based on earlier work[8]. The amplification is controlled by the length scale b_1 and power p_1, and the decay is controlled by length scale b_2 and power p_2. The noise source parameter vector is defined as:

$$\begin{aligned} A_1 &= \frac{U_c}{U_j} = \frac{\omega/\alpha}{U_j} \\ A_2 &= b_1 \\ A_3 &= b_2 \\ A_4 &= p_1 \\ A_5 &= p_2 \\ A_6 &= Q \end{aligned} \tag{25}$$

Constraints are placed on A_1 so that the convective velocity U_c is close to a target value ranging from $0.45U_j$ to $0.6U_j$, depending on the frequency. The wavenumber α is thus determined from the parameter A_1. The minimization process of Eq.23 used the Restarted Conjugate Gradient method of Shanno and Phua[23] (ACM TOM Algorithm 500).

Results for Mach 0.9 jet

Parameterization of the wavepacket requires judicious choices for the helical mode and a reasonable constraint for the convective velocity ratio U_c/U_j. Experimentation with the minimization process of Eq. 23 shows that, for given frequency, there are one or two helical modes that can fit the experimental results very well, while for other modes it is impossible to get a good fit regardless of the parameter values. For example, for Sr=0.2 mode n=0 works best; for Sr=0.5, n=1; and for Sr=1.0, n=2. The predominance of modes n=0,1, and 2 for this range of Strouhal numbers is in line with results of helical microphone measurements on similar jets by Juve *et al.*[24] and by Brown and Bridges[25]. In general, it is found that a higher helical mode is needed with increasing frequency.

The other consideration is the convective velocity ratio U_c/U_j, which here is set to range between 0.45 (low frequency) to 0.6 (high frequency). As mentioned earlier, U_c/U_j was the only constraint in the cost function. Figures 5, 6, and 7 show parameterization results for Strouhal numbers Sr=0.2, 0.5, and 1.0, respectively. Plotted are the real part of the wavepacket shape $p_0(x)$ and the modeled and experimental intensity distributions versus polar angle. The experimental distribution is the measured sound pressure level at the particular Strouhal number. The plots include the parameter values, with Q_{rel} denoting the relative contribution of the monopole to the radiated field.

With increasing frequency, the minimization scheme leads to smaller wavepacket widths. Note the increasing helical mode with higher frequency, which suggests that the azimuthal content of the source shifts to higher modes with increasing Strouhal number. In other words, matching of the experimental intensity distribution requires smaller width combined with higher helical mode as the frequency increases. Figures 5-7 demonstrate that good fits can be obtained between the modeled and experimental intensity polar distributions, with errors on the order of 0.1 dB.

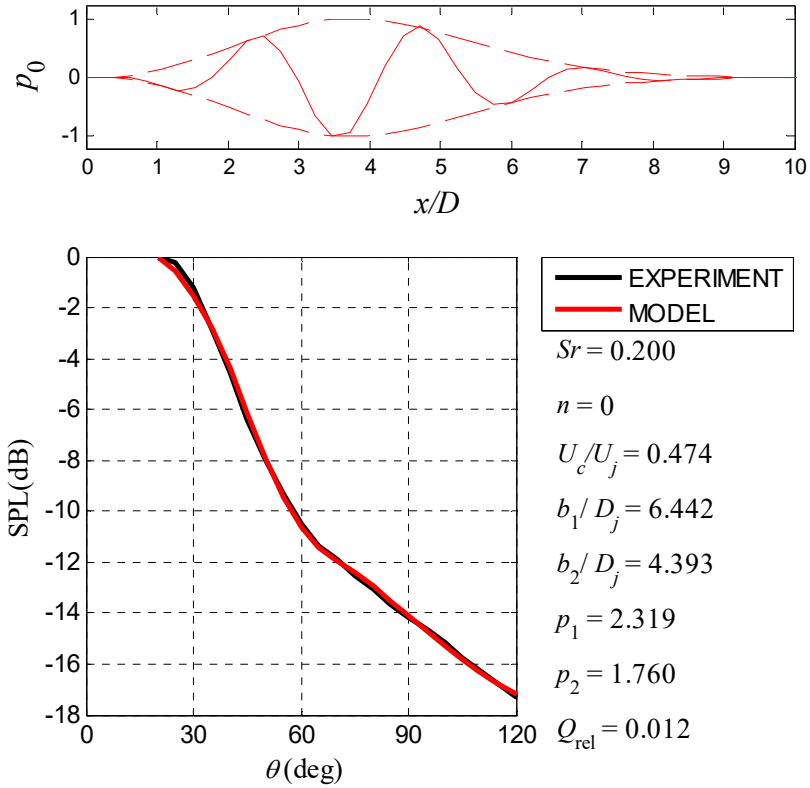

Fig. 5 Parameterization for Mach 0.9 cold jet at *Sr*=0.2. Helical mode *n*=0.

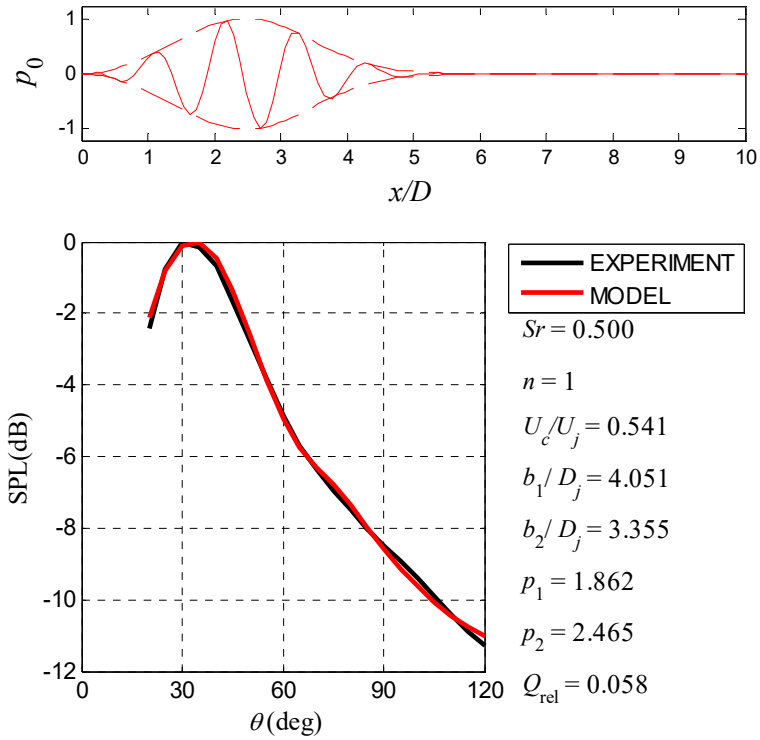

Fig. 6 Parameterization for Mach 0.9 cold jet at *Sr*=0.5. Helical mode *n*=1.

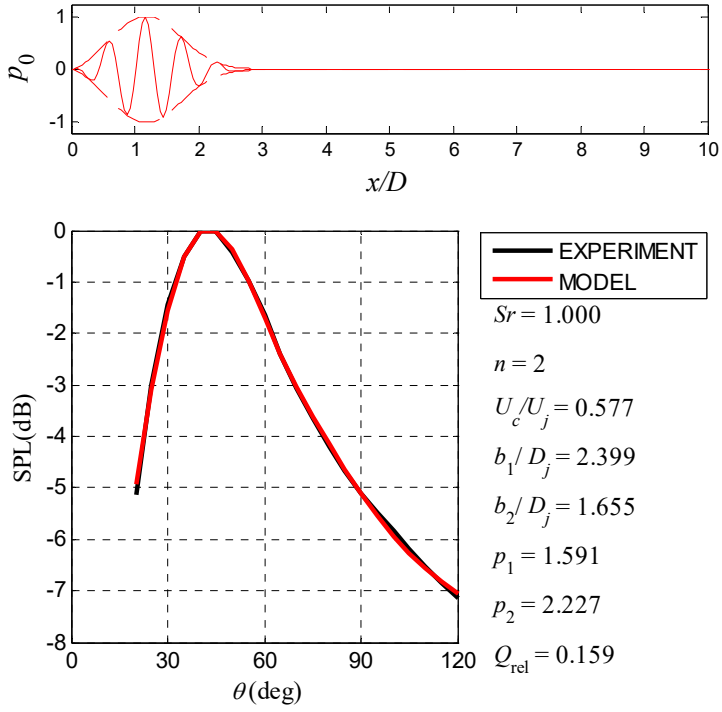

Fig. 7 Parameterization for Mach 0.9 cold jet at *Sr*=1.0. Helical mode *n*=2.

It is instructive to examine the radiative component of the wavepacket as given by Eq. 4. Figure 8 compares the real parts of the full wavepacket shape and its radiating component for the result of Fig. 7 (Sr=1). First, note that the amplitude of the radiating component is about a factor of 100 smaller than that of the full waveform. The radiating component is much more extended axially and has irregular shape - it is not exactly an amplitude-modulated sinusoidal perturbation – due to the "sinc" convolution of Eq. 4. The extended nature of the radiating source may have implications on the scattering of the wavepacket-emitted field from solid surfaces, a problem of relevance to the shielding and reflection of jet noise[8]. Note that the hydrodynamic component, given by Eq. 3a evaluated at r=r_0, is also more extended than the prescribed wavepacket source. The prescribed wavepacket source consists of the superposition of the radiating and hydrodynamic components.

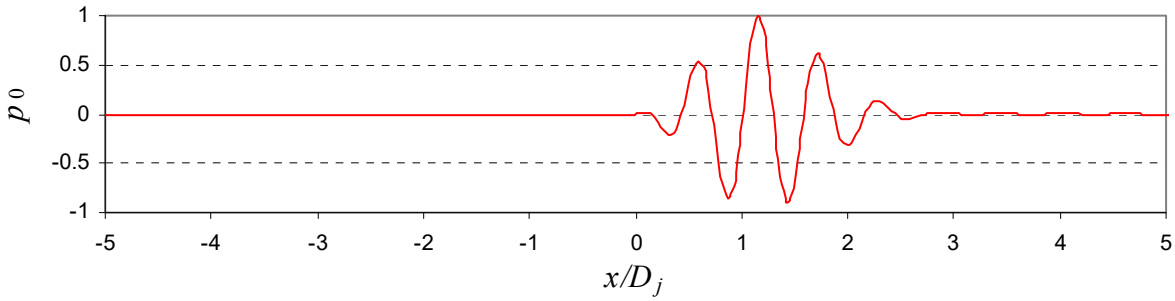

(a)

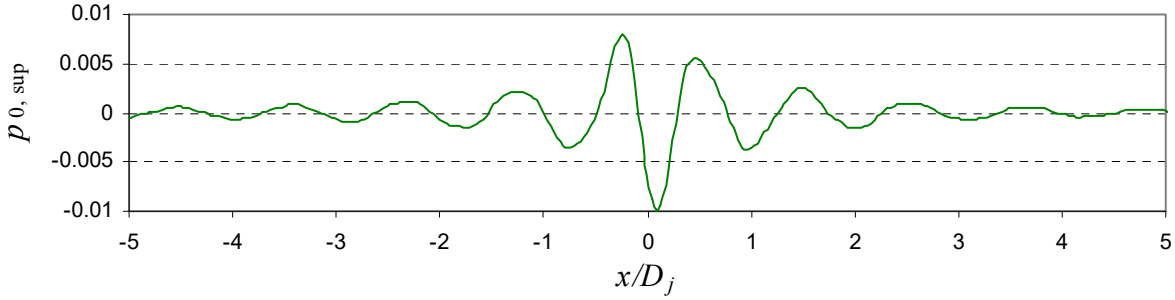

(b)

Fig. 8 Comparison of (a) the full waveform and (b) its radiating component for the wavepacket of Fig.7.

B. Global Parameterization

Approach

The preceding methods dealt with determination of the noise source parameters for a given frequency. The global parameterization procedure pertains to estimating the source parameters at all frequencies of interest using a single minimization scheme. It is based on prescription of general trends versus frequency for the wavepacket and monopole parameters. Central to this scheme is the *self-similar* wavepacket formulation of Section II.B.

The source parameters are now given as functions of frequency ω, using the parameter vector B_k and the relations:

$$\frac{U_c}{U_j} = B_1 \tanh(B_2 \omega^{0.3})$$
$$b_1 = \frac{B_3}{\omega}$$
$$b_2 = \frac{B_4}{\omega} \tag{26}$$
$$p_1 = B_5$$
$$p_2 = B_6$$
$$Q = B_7 \tanh(B_8 \omega)$$

The tanh trend for the convective velocity comes from the expectation that, at low frequency (typically Strouhal numbers less than 0.1), noise comes from the region past the potential core where the velocity (and consequently the ratio U_c/U_j) decays. As the frequency increases, the noise source location tends toward the potential-core region where the $U_c \approx$ constant. The particular form for U_c/U_j comes from experience using the elementary wavepacket model. The expressions for the widths b_1 and b_2 are consistent with the self-similar concept of the wavepacket where the width is inversely proportional to frequency. Finally, the monopole strength Q displays a tanh trend with frequency based on experience using the standard parameterization approach.

Helical mode versus frequency

A critical aspect of the global parameterization scheme is a reasonable prescription for the dominant helical mode versus frequency. It was noted earlier that higher modes are required to match the jet directivity with increasing frequency. Here we try to put this observation on a quantitative basis. Refer to the solution for the variance for the self-similar wavepacket, Eq. 19. The polar direction of peak emission (where S_w is maximixed at given frequency) is obtained by differentiating Eq.19 with respect to the polar angle θ, resulting in:

$$\frac{d}{d\theta} \frac{\left| \hat{P}_0\left(M_c \cos\theta\right) \right|}{\left| H^{(1)}_{n(\omega)}\left(\frac{\omega}{a_\infty} r_0 \sin\theta \right) \right|} = 0 \tag{27}$$

For a given universal wavepacket funtion $P_0(\xi)$, Eq. 27 gives the direction of peak emission θ_{peak} as a function of frequency ω and helical mode $n(\omega)$. Figure 9 shows such as solution on the polar angle - Strouhal number plane. For each helical mode n, the blue line defines the locus of θ_{peak} versus frequency. Overlaid on the diagram is the experimental direction of peak emission. The intersection of the theoretical curves with the experimental curve define the helical mode number versus frequency. It is seen that, as the frequency increases, progressively higher modes are needed to match the experimental directivity. Aside from its practical value, the process illustrated by Fig. 9 indicates a strong connection between helical mode content and directivity of jet noise. Figure 10 plots a representative distribution of the helical mode versus Strouhal number. The trend for $Sr > 0.5$ is almost linear.

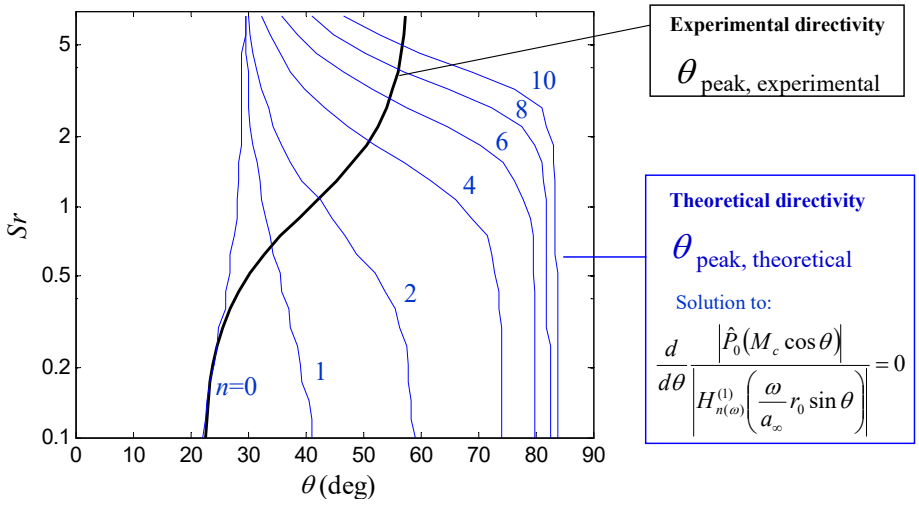

Fig. 9 Determination of helical mode versus frequency.

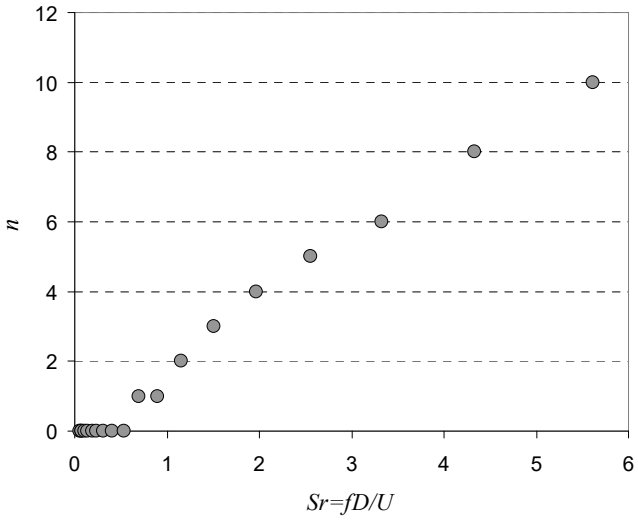

Fig. 10 Representative variation of the helical mode *n* versus Strouhal number.

Cost function

We seek parameters B_k (8 parameters for the scheme of Eq. 26) that minimize the difference, in a least-squared sense, of the modeled and experimental autospectra for all the polar angles and frequencies (Strouhal numbers) of interest. In analogy with Eq. 23, the cost function becomes:

$$F(\mathbf{B})=\sqrt{\frac{1}{N_q N_j}\sum_{q=1}^{N_q}\sum_{j=1}^{N_j}\left[L_{\exp}(\theta_j,\omega_q)-L_{\text{mod}}(n_q,\mathbf{B},\theta_j,\omega_q)\right]^2+\sum_{k=1}^{K}C_k\left(B_k-B_{k,\text{target}}\right)^2} \tag{28}$$

where θ_j, j=1,.., N_j are the polar angles of interest and ω_q, q=1,.., N_q are the frequencies of interest. As with the standard cost function of Eq. 23, we constrain selected parameters to fall within a certain range through the second term in the cost function. In this study only the parameter B_1, governing the convective velocity ratio, was constrained.

To determine the helical modes n_q using the process of Eq. 27, we need a reasonable choice for the universal wavepacket shape $P_0(\xi)$. We determine this shape by applying Eq. 28 at a single frequency - essentially reducing it to Eq. 23. The frequency should be high enough that the self-similar assumption

is valid - typically Strouhal number at or above 0.5. We minimize the cost function for a variety of helical modes, and select the mode (and associated model parameters, $B_1,...,B_8$) that provide the best match between modeled and experimental intensities for that frequency. Now that we have the desired wavepacket shape, we apply the helical-mode-determination scheme of Eq. 27. Once the modes are determined, the global minimization process of Eq. 28 is applied for all the frequencies of interest.

Results for Mach 0.9 jet

Figure 11 shows results of the global parameterization of the Mach 0.9 jet, using two conditions. In the first condition, the parameterization was performed for the wavepacket alone, setting the monopole strength to zero. In the second condition, the monopole strength was included in the parameters. Each subfigure depicts contour plots of the experimental and modeled spectra, as well as line plots of the modeled spectrum at polar angles θ=25° and θ=90°.

Examining the predictions for the wavepacket alone, Fig. 11a, we see that the main features of the spectrum are matched but there are quantitative discrepancies in low θ - high Sr corner of the spectrum. The broadening of the spectrum with increasing polar angle is unquestionable. This is significant. A single noise source - the wavepacket - creates a narrow spectrum at small angles and a wide spectrum at large angles. The spectral change comes from the Hankel function term discussed previously, in conjunction with the helical-mode determination of Eq. 27. Even though this result does not preclude an additional source broadening the spectrum, it shows that a two-source model is not necessary to explain the variation of the spectrum with polar angle.

Including the monopole, Fig. 11b, allows a very good match between the modeled and experimental spectra. The error, as measured by the cost function of Eq. 28, is on the order of 1 dB. The monopole may represent, in a very simple way, the "incoherent" noise source of the two-source model. Alternatively, it may represent a noise source associated with real effects such as reflections from the nozzle lip or nozzle surface. It is clear that addition of the monopole does not change the conclusion of the previous paragraph. Slight irregularities in the shapes of the spectra are numerical artifacts and do not represent any physical processes.

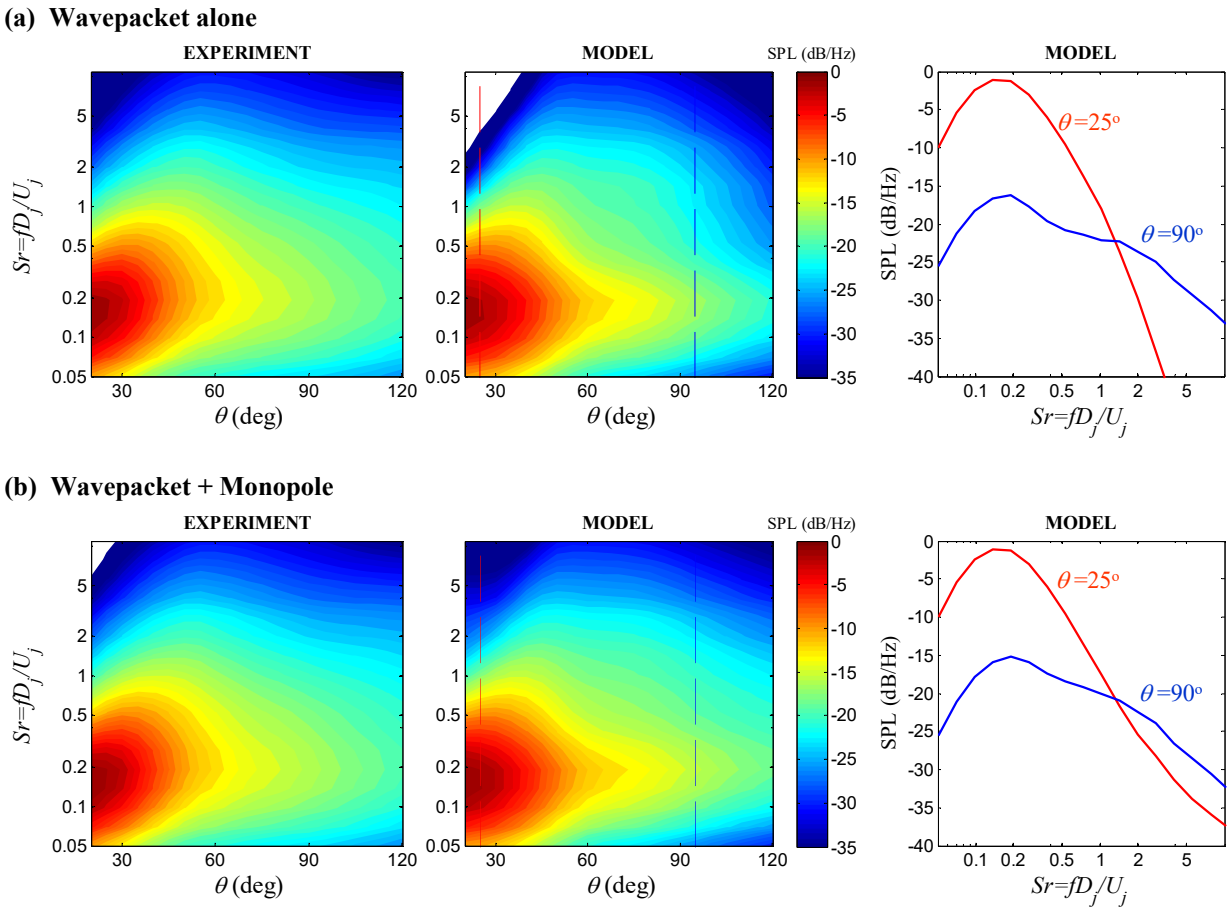

Fig. 11 Results of the global parameterization for Mach 0.9 cold jet using (a) wavepacket alone source model and (b) wavepacket combined with monopole. Contour plots compare the experimental and modeled sound pressure level (SPL) spectra. Line plots indicate the modeled SPL at polar angles of 25º and 90º.

V. Concluding Remarks

Whereas previous experimental studies have focused on investigating the noise source at a small number of frequencies (typically near the Strouhal number of peak emission), the present study underscores the importance and benefits of looking at the entire spectrum of jet noise as illustrated in Fig.1. In particular, the directivity-versus-frequency trend provides new insights into the helical content of the noise source.

This study demonstrated that a significant amount of information can be inferred from the far-field spectrum, particularly from its directivity, that enables construction of a wavepacket with reasonable physical characteristics. To construct the noise source model for a given frequency, the wavepacket is parameterized and the parameters are determined by least-squares minimization of the difference between the modeled and experimental sound intensity distributions in the far field.

The parameterization process can be applied simultaneously to all frequencies of interest through the concept of the self-similar wavepacket, i.e., a wavepacket with universal shape whose axial scale varies inversely with frequency. A stochastic extension of this concept shows a connection between the shape of the far-field spectrum and the emission polar angle. This relation indicates that the broadening of the spectrum with increasing polar angle can be explained on the basis of a single noise source (the wavepacket), rather than the prevailing model of two disparate noise sources, one coherent and the other incoherent.

The generic wavepacket shape used in this study is expected to work adequately for other jets of the same class as the one treated here, namely single-stream round jets without shock-cell noise. Nevertheless, the model presented here is a simple formulation that needs to be further extended. Future enhancements need to include the finite azimuthal coherence of the source and allow a richer azimuthal mode content at a given frequency. Applications to the near field must include the stochastic nature of the wavepacket origin x_0 in Eq. 13.

Acknowledgment

The author considers his association and collaboration with Professor Dennis K. McLaughlin a distinct honor and privilege. The opportunity to contribute to this special issue of IJA celebrating the lifetime achievements of Professor McLaughlin is highly appreciated. The research presented in this paper was funded by Boeing Subcontract No. 208547 in support of NASA contract NNL07AA54C "Acoustic Prediction Methodology and Test Validation for an Efficient Low-Noise Hybrid Wing Body Subsonic Transport."

References

1. McLaughlin, D.K., and McColgan, C.J., "Hot-Wire Measurements in a Supersonic Jet at Low Reynolds Numbers," AIAA Journal, Vol. 12, No. 9, Sep. 1974, pp. 1279-1981.
2. McLaughlin, D.K., Morrison, G.L., and Troutt, T.R., "Experiments on the Instability Waves in Supersonic Jet and Their Acoustic Radiation," *Journal of Fluid Mechanics*, Vol. 69, No.1, 1975, pp. 73-95.
3. Tam, C.K.W., "Directional Acoustics Radiation from a Supersonic Jet Generated by Shear Layer Instability," *Journal of Fluid Mechanics*, Vol. 46, No.4, 1971, pp. 757-768.
4. McLaughlin, D.K., Morrison, G.L., and Troutt, T.R., "Reynolds Number Dependence in Supersonic Jet Noise," *AIAA Journal*, Vol. 15, No.4, Apr. 1977, pp. 526-532.
5. Troutt, T.R., and McLaughlin, D.K., "Experiments on the Flow and Acoustic Properties of a Moderate-Reynolds-Number Supersonic Jet," *Journal of Fluid Mechanics*, Vol. 116, 1982, pp. 123-156.

6. Brown, G.L., and Roshko, A., "On Density Effects and Large Structure in Turbulent Mixing Layers," *Journal of Fluid Mechanics*, Vol. 64, No.4, 1974, pp. 775-816.

7. Russell, J., and Berton, J., "Stone Jet Noise Module (ST2JET)", ANOPP Theoretical Manual, ver.25, NASA Langley Research Center, Hampton, VA, 2006.

8. Papamoschou, D., "Prediction of Jet Noise Shielding," AIAA Paper 2010-0653, Jan. 2010.

9. C.K.W. Tam, K. Viswanathan, K.K. Ahuja, J. Panda, J., "The sources of Jet Noise: Experimental Evidence", *Journal of Fluid Mechanics*, Vol. 615, 2008, pp. 253-292.

10. Papamoschou, D., "Wavepacket Modeling of the Jet Noise Source," AIAA Paper 2011-2835, June 2011.

11. Papamoschou, D., "Imaging of Distributed Directional Noise Sources," *Journal of Sound and Vibration*, Vol. 330, No.10, 2011, pp. 2265-2280.

12. Bonnet, C.M.T., and Fisher, J., "Correlation Techniques and Modal Decomposition Analysis for the Detection of Azimuthally Coherent Structures in Jet Flows," *Journal of Sound and Vibration*, Vol. 66, No.4, October 1979, pp.545-555.

13. Tam, C. K. W., and Burton, D. E., "Sound Generation by the Instability Waves of Supersonic Flows. Part 2. Axisymmetric Jets," *Journal of Fluid Mechanics*, Vol. 138, 1984, pp. 273-295.

14. Crighton, D.G. and Huerre, P., "Shear-Layer Pressure Fluctuations and Superdirective Acoustic Sources," *Journal of Fluid Mechanic*s, Vol. 220, 1990, pp. 355-368.

15. Avital, E.J., Sandham, N.D., and Luo, K.H., "Mach Wave Radiation by Mixing Layers. Part I: Analysis of the Sound Field," *Theoretical and Computational Fluid Dynamics*, Vol. 12, 1998, pp. 73-90.

16. Morris, P.J., "A Note on Noise Generation by Large Scale Turbulent Structures in Subsonic and Supersonic Jets," *International Journal of Aeroacoustics*, Vol. 8, No. 4, 2009, pp. 301-316.

17. Reba, J., Simonich, J., and Schlinker, R., "Sound Radiated by Large-Scale Wave-Packets in Subsonic and Supersonic Jets," AIAA Paper 2009-3256, May 2009.

18. Reba, R., Narayanan, S., and Colonius, T., "Wave-Packet Models for Large-Scale Mixing Noise," *International Journal of Aeroacoustics*, Vol. 9, No. 4-5, pp. 533-558, 2010.

19. Jordan, P. and Colonius, T. "Wave Packets and Turbulent Jet Noise," Annual Review of Fluid Mechanics, Vol. 45, Jan. 2013, pp. 173-195.

20. Cavalieri, A.V.G., Rodriguez, D., Jordan, P., and Colonius, T., "Wavepackets in the Velocity Field of Turbulent Jets," *Journal of Fluid Mechanics*, Vol. 730, Sep. 2013, pp. 559-592.

21. Chan, Y.Y., "Spatial Waves in Turbulent Jets," *Physics of Fluids*, Vol. 17, No. 1, 1974, pp. 46-53.

22. Fuchs, H.V. and Michalke, A., "Introduction to Aerodynamic Noise Theory," *Progress in Aerospace Sciences*, Vol. 14, 1973, pp. 227-297.

23. Shanno, D.F., and Phua, K.H., "Minimization of Unconstrained Multivariate Functions," *ACM Transactions on Mathematical Software*, Vol. 6, No.4, 1980, pp. 618-622.

24. Juve, D., Sunyach, M., and Comte-Bellot, G., "Filtered Azimuthal Correlations in the Acoustic Far Field of a Subsonic Jet," *AIAA Journal*, Vol. 17, No.1, 1979, pp. 112-113.

25. Brown, C., and Bridges, J., "Acoustic Efficiency of Azimuthal Modes in Jet Noise Using Chevron Nozzles", AIAA Paper 2006-2654, Jan. 2006.